Osteoarthritis and Cartilage 19 (2011) 700–710

Osteoarthritis and Cartilage

OARSI OSTEOARTHRITIS RESEARCH SOCIETY INTERNATIONAL

Evaluation of translation in the normal and dysplastic hip using three-dimensional magnetic resonance imaging and voxel-based registration

K. Akiyama †, T. Sakai ‡*, J. Koyanagi †, H. Yoshikawa ‡, K. Sugamoto †

† *Dept. of Orthopaedic Biomaterial Science, Osaka University Graduate School of Medicine, Suita, Japan*
‡ *Dept. of Orthopaedic Surgery, Osaka University Graduate School of Medicine, Suita, Japan*

ARTICLE INFO

Article history:
Received 29 July 2010
Accepted 28 January 2011

Keywords:
Translation
Instability
Dysplasia
Voxel-based registration
Magnetic resonance imaging

SUMMARY

Objective: To elucidate *in vivo* hip instability by comparing normal hips to hips with acetabular dysplasia by evaluating three-dimensional (3D) translations of the femoral head center (FHC) at different hip positions using magnetic resonance imaging (MRI).

Design: Forty normal hips and 22 dysplastic female hips were examined. MRI was performed at four different positions bilaterally: neutral, 45° of flexion, 15° of extension, and the Patrick position. Femoral and pelvic bones were separately extracted at the neutral position and superimposed over the images of each different position using voxel-based registration. The distance between the acetabular center and FHC at neutral position was defined as 3D-migration. The distance between FHC at neutral position and that at each different position was defined as 3D-translation. Two-way repeated measures analysis of variance was performed to consider the dependency between right and left-side data, and multiple linear regression analyses were performed to assess independent relationships.

Results: The center-edge (CE) angle was the determinant for 3D-migration ($\beta = -0.415$, $P = 0.001$), and there was a statistical significant difference in 3D-migration between normal female hips and dysplastic hips ($P = 0.047$). From neutral to the Patrick position, the FHC of normal and dysplastic hips translated postero-infero-medially by 1.12 ± 0.39 mm (0.45–1.85 mm) and 1.97 ± 0.84 mm (0.95–4.34 mm), respectively, and the difference between the groups was statistically significant ($P = 0.005$). CE angle was the determinant for 3D-translation from neutral to the Patrick position ($\beta = -0.730$, $P < 0.001$). The average root mean square error in 3D-translation was 0.172 mm and 0.193 mm for intra- and interobserver reproducibility, respectively.

Conclusions: Hip instability was increased in proportion to the severity of acetabular dysplasia. A 3D MRI voxel-based registration technique can show *in vivo* morphology and kinematics of the native hip without exposure to radioactivity.

Introduction

Acetabular dysplasia has been implicated in the development of secondary osteoarthritis (OA) of the hip[1,2]. Dysfunction of the hip secondary to dysplasia could derive from multifactorial problems including excessive stresses on the articular cartilage[3,4] and dynamic hip instability[5,6]. An insufficient biomechanical environment of increasing contact stress for the acetabulum or femoral head due to reduced contact area has been indicated[1,7,8]. Concerning hip instability, however, there have been a few *in vitro*[9,10] and *in vivo*[5,11] studies. Studies have evaluated native hip joint kinematics with accelerometry with skin markers[5] and magnetic resonance imaging (MRI) with surface registration[12]. Evaluation of dynamic hip instability may elucidate causes of secondary OA and unveil the etiology of primary hip OA.

In the present study, a unique technique was developed for direct *in vivo* measurement of human joint motion using three-dimensional (3D) MRI with voxel-based registration[13–15]. This technique enables analysis and visualization of hip joint motion. The purpose of the present study was to determine *in vivo* 3D motion of the normal hip joint and of hips with acetabular dysplasia by evaluating hip joint translation, and to validate the evaluation of hip joint translation using this novel method.

* Address correspondence and reprint requests to: Takashi Sakai, Dept. of Orthopaedic Surgery, Osaka University Graduate School of Medicine, 2-2 Yamadaoka, Suita 565-0871, Japan. Tel: 81-6-6879-3552; Fax: 81-6-6879-3559.
E-mail address: tsakai-osk@umin.ac.jp (T. Sakai).

1063-4584/$ – see front matter © 2011 Osteoarthritis Research Society International. Published by Elsevier Ltd. All rights reserved.
doi:10.1016/j.joca.2011.01.017

Methods

Patients and study design

Twenty-two volunteers (10 males and 12 females; mean age 30.4 years) without history of hip pain or any hip disease and 13 patients (all females; mean age 31.6 years) who had bilateral or unilateral dysplastic hips at pre- or early stages of OA (Tönnis grade ≤ 1)[16] were recruited. Radiographs were not taken in any volunteers to minimize exposure to radiation. MRI was carried out in all individuals and the center-edge (CE) angle on the mid-coronal MR image was available for comparison[17]. Criteria for presence of acetabular dysplasia and enrollment in this study were as follows: radiological evidence of dysplasia with a CE angle $<20^\circ$ on anteroposterior radiographs[18]; Group I subluxation according to the classification of Crowe *et al.*[19]; no radiological evidence of joint space narrowing; no radiological deformity of the femoral head; and no previous operation on the hip joint. We also excluded the individual whose bilateral hips could not be classified into the same category (normal or dysplasia) for the precise statistical analysis. The bilateral hips (four hips) of two female volunteers that exhibited a CE angle $<20^\circ$ on the mid-coronal MR image were enrolled as dysplastic hips. Four patients were excluded because of one unilateral postoperated hip, one unilateral normal hip, and two unilateral deformed femoral heads with the contralateral normal hip. Finally, 22 hips were enrolled as dysplastic hips while 40 hips were normal hips (Table I). The dysplastic hips were disproportionately all females because in Japan, hip dysplasia is common, especially in females, and causes approximately 90% of all hip OA[20]. This study was approved by the local institutional review board. All subjects gave informed consent to participate; if the subject was under 20 years of age, informed consent was obtained both from the subject and the subject's parents.

3D MRI was performed using a flexible surface body coil on a 1.5-T MR system (MAGNETOM Espree, Siemens, Erlangen, Germany). The following three sequences were preliminarily tried in a healthy hip joint: true fast imaging with steady-state precession (TrueFISP) [repetition time (TR)/echo time (TE); 4.96/2.13 ms]; fast low-angle shot (FLASH) (TR/TE; 17.00/9.40 ms); volumetric interpolated breath-hold sampling (VIBE) with fat saturation (TR/TE; 15.30/6.67 ms). The TrueFISP was selected for high image contrast[21] and for higher values of the normalized cross-correlation (NCC)[22,23] between the images in voxel-based registration. Detailed parameters of the 3D TrueFISP were as follows: TR/TE, 4.96/2.13 ms; flip angle, 28°; section thickness, 1.0 mm; in-plane resolution, 1.0 mm; matrix, 384×384; imaging direction, coronal. Imaging time was 3 min 26 s [Fig. 1].

Subjects were placed in a supine position and each hip was maintained in the center of the magnet bore at all positions. Images were made with the hip in four different positions bilaterally using a non-magnetic movable device made from non-ferromagnetic materials with Velcro tape: neutral, 45° of flexion, 15° of extension, and the Patrick position[24] which was 50° of flexion, 40° of abduction, and 60° of external rotation. Thus, MR images were acquired four times per hip joint [Fig. 2].

Data were saved in a standard digital imaging and communications in medicine (DICOM) format and imported into the Virtual Place-M software (Medical Imaging Laboratory, Tokyo, Japan) on a Dell Precision T3400 workstation (Dell Inc., Round Rock, TX) for segmentation and voxel-based registration. The system was run on an Intel Core2 Duo computer, 3.0 GHz, 2.0 Gb RAM, under Windows XP Professional edition. All data were analyzed by an author (KA).

Table I
Comparison of clinical and morphological features

	Normal male hips ($N = 20$)	Normal female hips ($N = 20$)	Dysplastic hips ($N = 22$)
Age (years)	29.8 ± 6.8	31.8 ± 7.5	32.9 ± 13.6
Weight (kg)	70.4 ± 7.2†	51.6 ± 7.3	52.9 ± 6.1
Height (m)	1.72 ± 0.05†	1.58 ± 0.04	1.59 ± 0.05
BMI (kg/m^2)	23.8 ± 2.1*	20.7 ± 3.0	20.8 ± 1.7
CE angle (°)	25.0 ± 3.9	27.9 ± 4.6	13.5 ± 5.3**
Femoral head radius (mm)	24.7 ± 0.8†	21.6 ± 1.0	22.2 ± 1.0
Acetabular sphere radius (mm)	28.0 ± 0.7†	24.6 ± 1.2	26.5 ± 1.7**
3D-migration (mm)	1.45 ± 0.56	1.35 ± 0.48	1.84 ± 0.74‡
3D-migration-*x* (mm)	−0.78 ± 0.39	−0.66 ± 0.28	−0.62 ± 0.57
3D-migration-*y* (mm)	−0.14 ± 0.57	0.28 ± 0.49	0.64 ± 1.15
3D-migration-*z* (mm)	−0.78 ± 0.86	−0.84 ± 0.73	−0.86 ± 0.90
3D-MP (%)	2.94 ± 1.16	3.12 ± 1.13	4.15 ± 1.71
3D-MPx (%)	−1.58 ± 0.79	−1.53 ± 0.66	−1.40 ± 1.26
3D-MPy (%)	−0.27 ± 1.14	0.66 ± 1.14	1.48 ± 2.63
3D-MPz (%)	−1.61 ± 1.75	−1.93 ± 1.72	−1.96 ± 2.03

Values are mean ± standard deviation.
The direction of the connecting line between the acetabular center (AC) (the origin) and the femoral head center (FHC) was divided into a 3D vector, and each value of the *x*-, *y*-, and *z*-axes element was divided by the diameter of the femoral head, to produce 3D-MPx (%), 3D-MPy (%), and 3D-MPz (%). Each *x*-, *y*-, and *z*-axes pointed anteriorly, superiorly, and laterally, respectively.
* $P < 0.05$ for the comparison between normal male hips and normal female hips.
† $P < 0.01$ for the comparison between normal male hips and normal female hips.
‡ $P < 0.05$ for the comparison between normal female hips and dysplastic hips.
** $P < 0.01$ for the comparison between normal female hips and dysplastic hips.

Segmentation and 3D surface model creation

MR images were represented as a series of two-dimensional images in sagittal, coronal, and axial directions. For each slice at neutral position, both the hemipelvis and proximal femur were separately extracted semi-automatically from MR images using the Virtual Place-M software; this process was called "segmentation". The articular cartilage was not segmented.

For each subject, the 3D surface bone model was reconstructed from the segmented area of MR images using the Marching Cubes algorithm of the Visualization Toolkit (VTK) (Kitware Inc., New York, NY), which created triangle models of constant density surfaces from 3D MR images[25]. The algorithm uses a case table of edge intersections to describe how a surface cuts through each cube in a 3D data set. The mean model error of this method has been reported to be 3.92%[26]. The surface model was saved in VTK format and visualized using original software with all programs written in Visual C++ (Orthopedics Viewer; Osaka University, Suita, Japan)[27].

Voxel-based registration

Voxel-based registration, a method for determining relative positions between volumetric images at different coordinates, was performed using the Virtual Place-M software. Each segmented image was registered to its mate by maximizing the NCC[13,22,23], which is a measure of the correlation, as follows:$\mathrm{NCC} = \sum(I_1 - \bar{I}_1)(I_2 - \bar{I}_2)/(\sqrt{\sum(I_1 - \bar{I}_1)^2}\sqrt{\sum(I_2 - \bar{I}_2)^2})$, where I_1 and I_2 are the voxel intensities of the floating and reference images, respectively; $\bar{I}_1$ and $\bar{I}_2$ are the mean voxel intensities of the floating and reference images, respectively; and the calculations include all voxels within the segmented region.

All registrations were rigid body with six degree of freedom, trilinear interpolation creating isotropic voxels ($1.0 \times 1.0 \times 1.0$ mm), and a multiresolution approach from low to high resolution. At low resolution, both images were resampled at 1/2 number of voxels along each linear dimension. The initial search interval (step size) was ±5° and ±5 voxels corresponding to ±10, or ±5 mm for resolutions of 1/2, or full voxels, respectively. The step size was

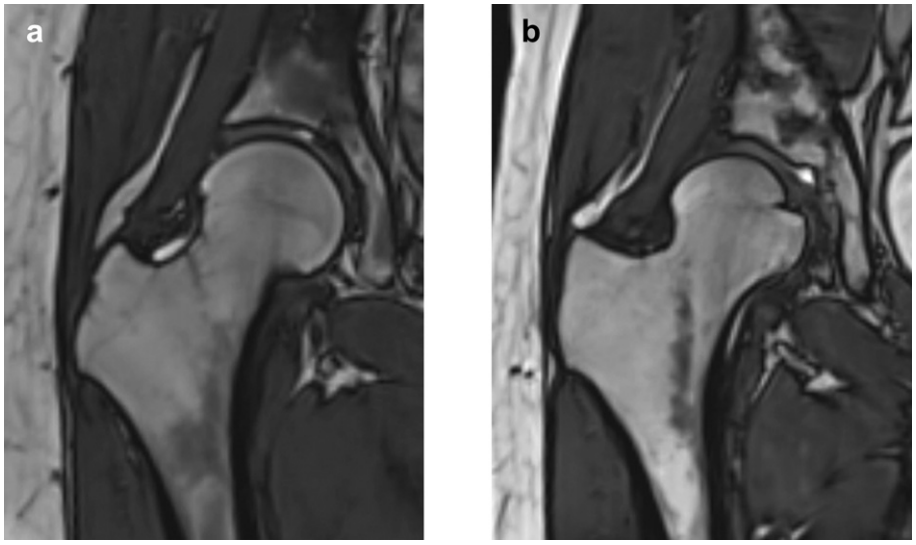

Fig. 1. Representative magnetic resonance images using TrueFISP (TR/TE, 4.96/2.13 ms; flip angle, 28°; section thickness, 1.0 mm; in-plane resolution, 1.0 mm; matrix, 384 × 384; imaging direction, coronal). (a) A right normal female hip. (b) A right dysplastic hip.

always reduced by a factor of 1/2. There were eight reductions for each resolution level. An iterative search was performed at each step size to vary the six rigid-body transformation parameters, setting maximum number of iterations at eight. The iterative search at each step size ended either when the maximum number of iterations was reached or the fractional change in NCC was smaller than 0.001. The steepest-descent method was used for optimization[28]. Accuracy of the voxel-based registration has been reported to be <0.52 mm in translation and 0.43° in rotation[13]. The mean computation time for the registration was 1 min 58 s for the femur and 1 min 38 s for the pelvis.

Motion analysis and definition of the local coordinate system

Let $M_p = [CS_p, C_p]$ and $M_f = [CS_f, C_f]$ be the coordinate system of the pelvis and femur at the neutral position, respectively (CS_p and CS_f are 3 × 3 rotation matrices and C_p and C_f are translation vectors). Let $T_p = [R_p, t_p]$ and $T_f = [R_f, t_f]$ be the rigid transformation applied to the pelvis and femur, respectively (R_p and R_f denote rotations while t_p and t_f denote translations). The hip joint transform is given by the matrix $T_{pf} = M_p^{-1} T_p^{-1} T_f M_f = [R_{pf}, t_{pf}]$ (R_{pf}, t_{pf} represent joint rotations and translations, respectively). This matrix can be converted to the three standard joint angles and shifts[12,29].

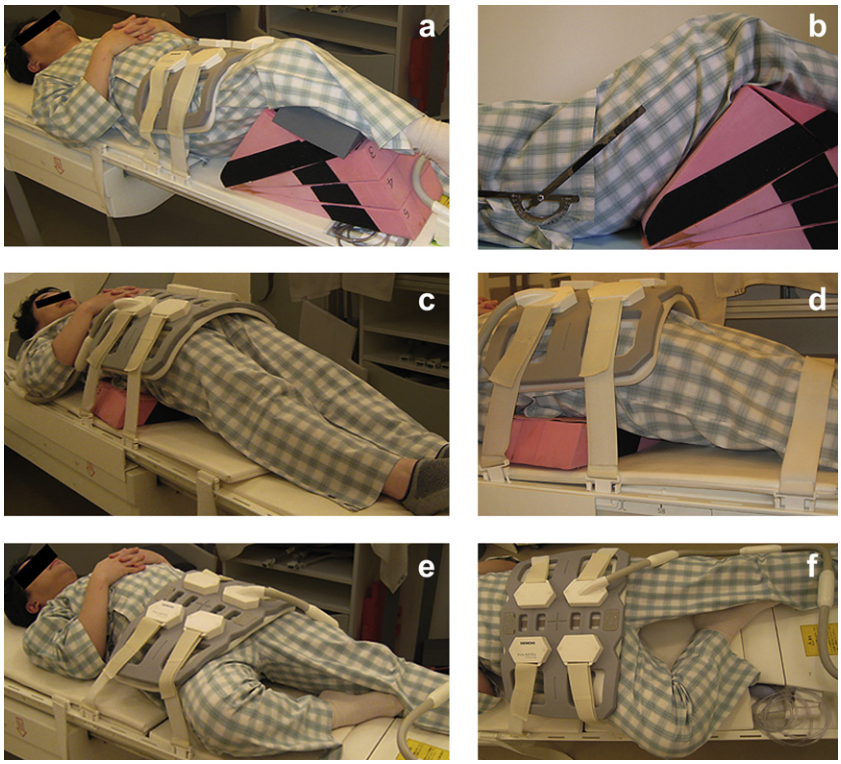

Fig. 2. Data acquisition of MRI using a non-magnetic movable device made from non-ferromagnetic materials. (a), (b) 45° flexion; (c), (d) 15° extension; (e), (f) The Patrick position.

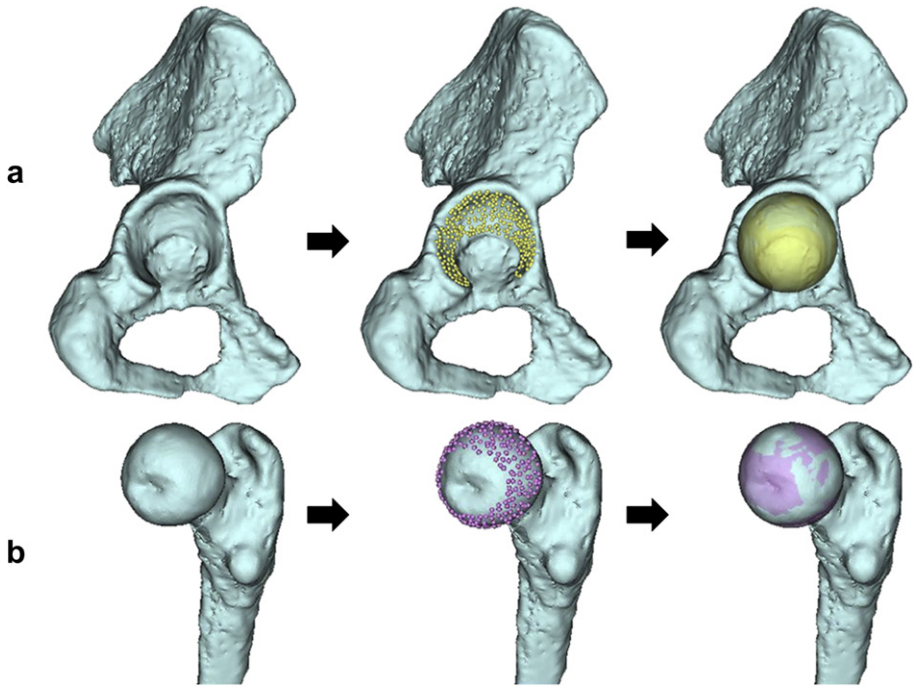

Fig. 3. Acetabular sphere and femoral head sphere. (a) 300 points were plotted on the subchondral bone of the acetabular lunate surface, and then the acetabular sphere was created automatically. (b) 300 points were plotted on the subchondral bone of the femoral head surface (except the fovea), and then the femoral head sphere was produced automatically.

On the articular subchondral bone surface of the femoral head (except the fovea) and of the acetabular lunate, 300 points were plotted to create the femoral head sphere and the acetabular sphere, respectively, with a least-square fitting of a sphere to a set of 300 points P_i given by the minimization of $\sum_{i\leq 300}(\|P_iC\| - r)^2$ where C is the center of the femoral head sphere, femoral head center (FHC), or the center of the acetabular sphere, acetabular center (AC), and r is the radius of the sphere [Fig. 3][12].

The distance between the AC and FHC at the neutral position was named 3D-migration, with the origin defined as the AC [Fig. 4]. The distance between the FHC at the neutral position and at each other position was named 3D-translation, with the origin defined as the FHC at the neutral position [Fig. 5]. 3D-migration and 3D-translation divided by the femoral head diameter were defined as the 3D-migration percentage (3D-MP) and 3D-translation percentage (3D-TP), respectively. The 3D direction of each connecting line between the AC and FHC or between the FHC at the neutral position and the FHC at each different position was evaluated [Figs. 4 and 5].

The *x*-, *y*- and *z*-axes were defined as orientation in the slice-encoding, phase-encoding, and frequency-encoding directions,

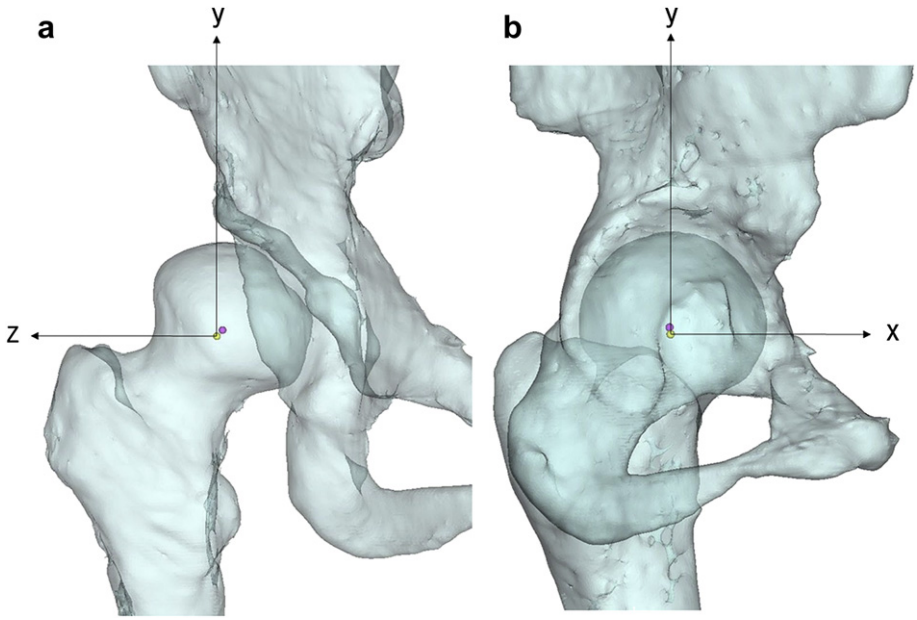

Fig. 4. 3D-migration in a right dysplastic hip. The distance between the yellow center of the acetabular sphere AC and the pink center of the femoral head sphere FHC was calculated as the 3D-migration, and the origin was defined as the AC. The direction of the connecting line is divided into 3D vector, *x*-axis element, *y*-axis element, and *z*-axis element pointing anteriorly, superiorly, and laterally, respectively. (a) Coronal plane view (YZ plane). (b) Sagittal plane view (XY plane).

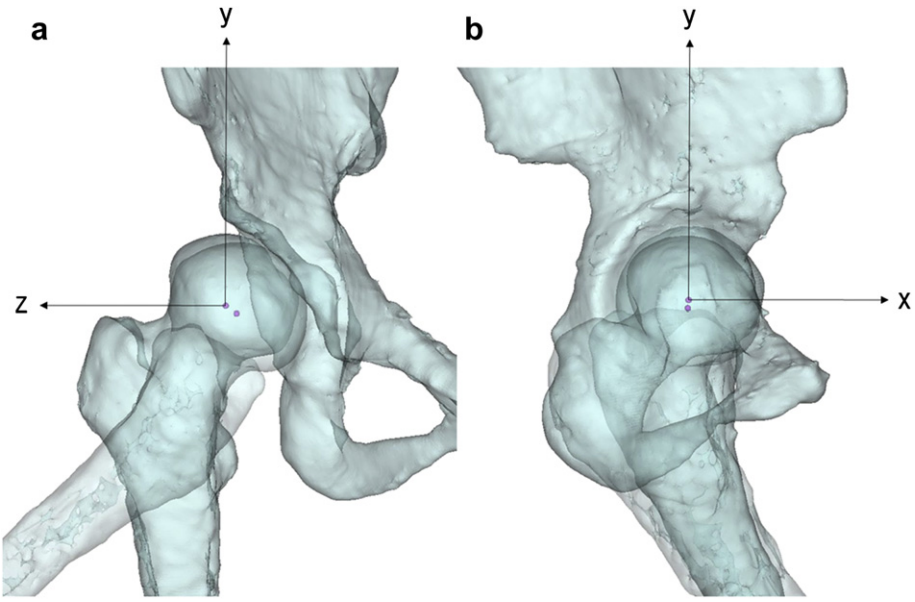

Fig. 5. 3D-translation from neutral to the Patrick position in a right dysplastic hip. The distance between the center of the femoral head sphere FHC at the neutral position and the FHC at the Patrick position was calculated as the 3D-translation from neutral to the Patrick position, with the origin defined as the FHC at the neutral position. The direction of the connecting line was divided into 3D vector with the *x*-axis, *y*-axis, and *z*-axis elements pointing anteriorly, superiorly, and laterally, respectively. (a) Coronal plane view (YZ plane). (b) Sagittal plane view (XY plane).

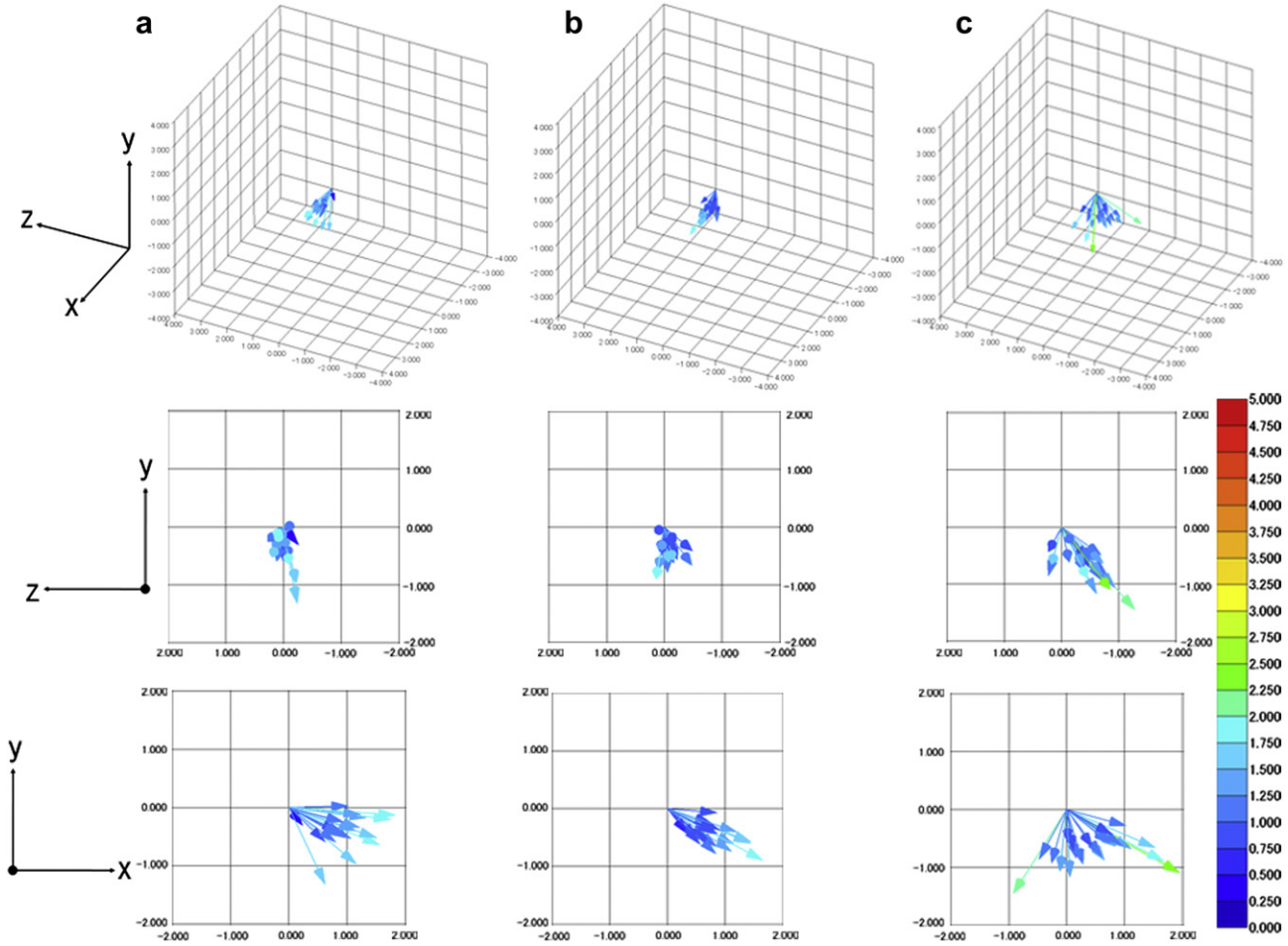

Fig. 6. The vectors of 3D-translation from neutral to 45° flexion. The *x*-axis, *y*-axis, and *z*-axis points anteriorly, superiorly, and laterally, respectively. Bird's-eye, coronal plane (YZ plane), and sagittal plane (XY plane) views are shown in (a) normal male hips, (b) normal female hips, and (c) dysplastic hips. The color scale is in millimeters.

respectively and pointed anteriorly, superiorly, and laterally, respectively. For simplification of the coordinate system, images of left hips were converted to their mirror images (right hips) by mirroring with respect to the mid-sagittal plane of the body.

Reproducibility test

To assess reproducibility, four healthy right hips (one male and three female subjects) were scanned using the same MRI protocol on two consecutive days. All MR data were segmented, registered, and analyzed twice by two authors (KA and JK) independently for intra- and interobserver reproducibilities. Data analysis sessions were performed with an interval of longer than a week. For each measurement of reproducibility, four-way comparisons between the two different days were performed for each parameter.

Statistical analysis

Because the gender-related comparisons are statistically and clinically independent of the comparisons between the normal female and the dysplastic patient, two-way repeated measures analysis of variance (RMANOVA) was performed in each comparison, with a split-plot design with the study group (normal male vs normal female, or normal female vs dysplasia) as the variable between groups and laterality as the variable within groups to consider the dependency between right and left-side data[30,31].

Linear regression analyses were performed in each hip position for the following parameters: age, body mass index (BMI), CE angle, femoral head radius, acetabular sphere radius, 3D-migration, 3D-translation, 3D-MP, and 3D-TP.

Multiple linear regression analyses were performed to assess independent relationships with 3D-migration and 3D-translation in 45° flexion, 15° extension, or the Patrick position as dependent variables, and age, sex, laterality, BMI, CE angle, femoral head radius, acetabular head radius, and 3D-migration as the explanatory variables. The selection criterion of variables for inclusion was forward-stepwise with an entrance criterion of $P < 0.05$ and an exit criterion of $P > 0.10$. The results of the model were presented using adjusted R^2. The variables in the final model were centralized to adjust for possible multicolinearity.

For each reproducibility measurement, intraclass correlation coefficients (ICC), the root mean square error (RMSE) and the mean error of measurement were assessed.

Statistical analyses were conducted using SPSS for Windows (version 19.0; IBM, Armonk, NY) and statistical significance was accepted for P values of <0.05.

Results

The standard deviation of the distance from the FHC to the 300 points on the bony surface of the femoral head was 0.36 ± 0.04 mm for normal male hips, 0.38 ± 0.04 mm for normal female hips, and 0.37 ± 0.05 mm for dysplastic hips. There were no statistical

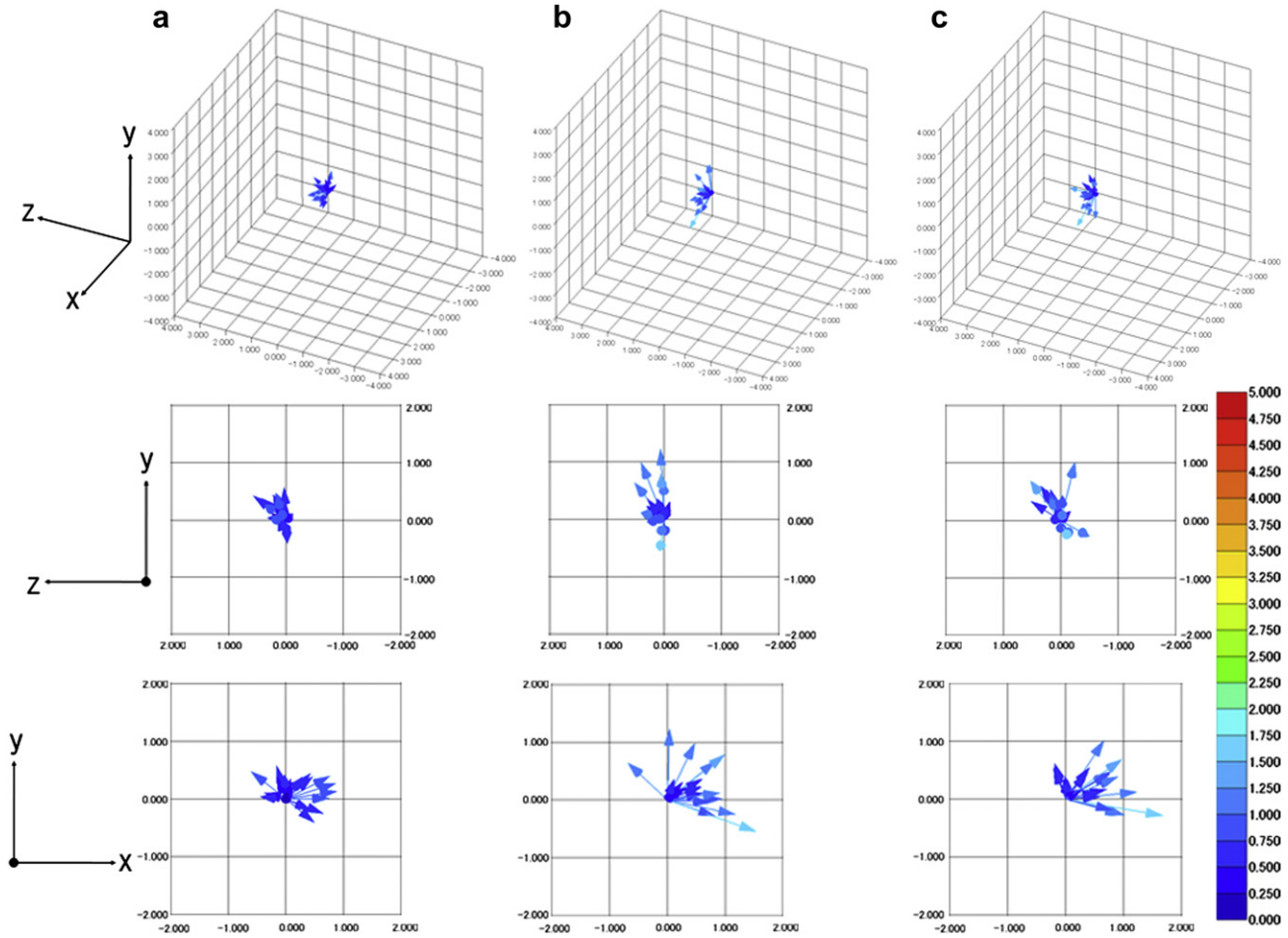

Fig. 7. The vectors of 3D-translation from neutral to 15° extension. The *x*-axis, *y*-axis, and *z*-axis points anteriorly, superiorly, and laterally, respectively. Bird's-eye, coronal plane (YZ plane), and sagittal plane (XY plane) views are shown in (a) normal male hips, (b) normal female hips, and (c) dysplastic hips. The color scale is in millimeters.

significant differences concerning spherical geometry of the femoral head between normal male hips and normal female hips ($P = 0.248$), or between normal female hips and dysplastic hips ($P = 0.760$).

The mean 3D-migration was 1.45 mm (range; 0.58–2.87 mm) for normal male hips, 1.35 mm (range; 0.65–2.41 mm) for normal female hips, and 1.84 mm (range; 0.38–3.55 mm) for dysplastic hips (Table I). Comparing normal female hips with normal male hips, there were statistical significant differences in weight, height, BMI, femoral head and acetabular sphere radius. Comparing normal female hips with dysplastic hips, there were statistical significant differences in CE angle ($P < 0.001$), acetabular sphere radius ($P = 0.006$), and 3D-migration ($P = 0.047$). Dysplastic hips tended to exhibit larger 3D-migration toward the superior direction than normal female hips.

The FHC tended to translate antero-inferiorly from neutral to 45° flexion [Fig. 6], anteriorly from neutral to 15° extension [Fig. 7], and postero-infero-medially from neutral to the Patrick position [Fig. 8] (Table II). The mean 3D-translation from neutral to 45° flexion was 1.27 mm (range; 0.45–1.91 mm) for normal male hips, 1.10 mm (range; 0.60–1.89 mm) for normal female hips, and 1.30 mm (range; 0.76–2.39 mm) for dysplastic hips [Fig. 6]. The mean 3D-translation from neutral to 15° extension was 0.61 mm (range; 0.24–0.98 mm) for normal male hips, 0.86 mm (range; 0.35–1.61 mm) for normal female hips, and 0.85 mm (range; 0.34–1.72 mm) for dysplastic hips [Fig. 7]. The mean 3D-translation from neutral to the Patrick position was 1.17 mm (range; 0.67–1.62 mm) for normal male hips, 1.12 mm (range; 0.45–1.85 mm) for normal female hips, and 1.97 mm (range; 0.95–4.34 mm) for dysplastic hips [Fig. 8]. Comparing normal female hips with dysplastic hips, there were statistical significant differences in 3D-translation ($P = 0.005$), 3D-translation-y ($P = 0.011$), 3D-translation-z ($P = 0.018$), 3D-TP ($P = 0.004$), 3D-TPy ($P = 0.012$) and 3D-TPz ($P = 0.018$) from neutral to the Patrick position [Fig. 8].

There was no correlation between clinical/morphological parameters and 3D-migration/3D-MP (Table III). From neutral to the Patrick position, strong negative correlations for dysplastic hips were found between CE angle and 3D-translation ($P < 0.001$; $r = -0.851$), and between CE angle and 3D-TP ($P < 0.001$; $r = -0.835$) (Table IV). There was no correlation between CE angle and 3D-translation ($P = 0.430$; $r = -0.187$) or between CE angle and 3D-TP ($P = 0.621$; $r = -0.118$) in normal female hips.

In multiple linear regression analyses, 3D-migration was negatively correlated with CE angle independently ($\beta = -0.415, P = 0.001$) (Table V). 3D-translation from neutral to 45° flexion was independently correlated with acetabular sphere radius ($\beta = 0.283$, $P = 0.012$). 3D-translation from neutral to 15° extension was independently correlated with sex ($\beta = 0.560$, $P < 0.001$) and BMI ($\beta = 0.438, P = 0.002$). CE angle most strongly explained the variation of 3D-translation from neutral to the Patrick position ($\beta = -0.730$, $P < 0.001$).

For intraobserver reproducibility, the mean ICC and mean RMSE were 0.893 and 0.172 mm for the 3D-translation value, respectively, and 0.926 and 0.199 mm for the 3D-translation vector (x, y, z),

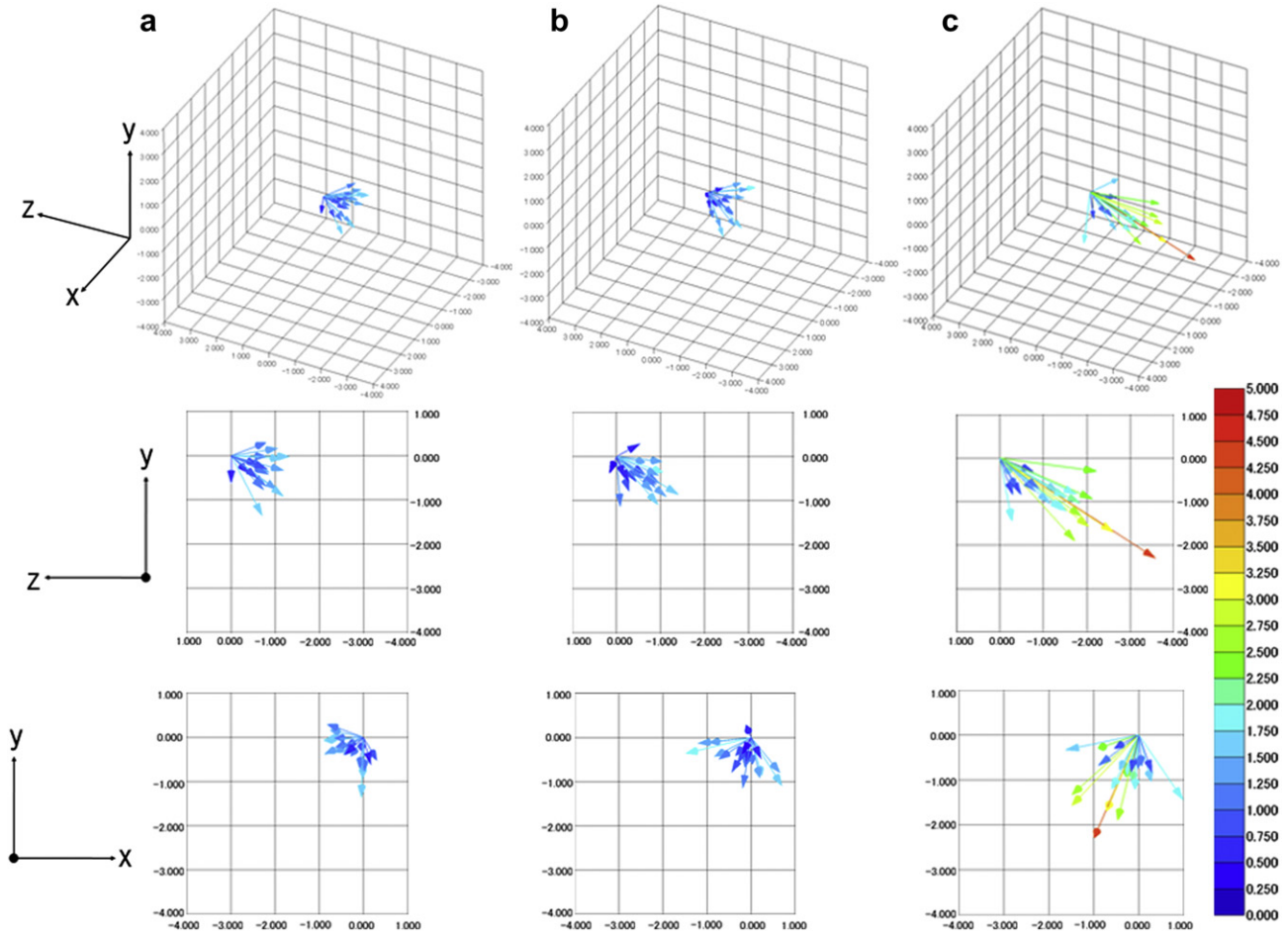

Fig. 8. The vectors of 3D-translation from neutral to the Patrick position. The x-axis, y-axis, and z-axis points anteriorly, superiorly, and laterally, respectively. Bird's-eye, coronal plane (YZ plane), and sagittal plane (XY plane) views are shown in (a) normal male hips, (b) normal female hips, and (c) dysplastic hips. The color scale is in millimeters.

Table II
Comparison of translation from neutral to each other position

	Normal male hips ($N=20$)	Normal female hips ($N=20$)	Dysplastic hips ($N=22$)
From neutral to 45° flexion			
3D-translation (mm)	1.27 ± 0.36	1.10 ± 0.31	1.30 ± 0.41
3D-translation-x (mm)	1.11 ± 0.41	0.92 ± 0.33	0.54 ± 0.70
3D-translation-y (mm)	−0.46 ± 0.32	−0.53 ± 0.19	−0.78 ± 0.26**
3D-translation-z (mm)	0.01 ± 0.15	−0.10 ± 0.18	−0.50 ± 0.38**
3D-TP (%)	2.56 ± 0.74	2.53 ± 0.65	2.91 ± 0.87
3D-TPx (%)	2.25 ± 0.84	2.12 ± 0.68	1.20 ± 1.54‡
3D-TPy (%)	−0.93 ± 0.64	−1.22 ± 0.43	−1.77 ± 0.59**
3D-TPz (%)	0.02 ± 0.31	−0.22 ± 0.40	−1.14 ± 0.86**
From neutral to 15° extension			
3D-translation (mm)	0.61 ± 0.20*	0.86 ± 0.34	0.85 ± 0.34
3D-translation-x (mm)	0.23 ± 0.45	0.57 ± 0.48	0.62 ± 0.47
3D-translation-y (mm)	0.21 ± 0.27	0.29 ± 0.43	0.27 ± 0.34
3D-translation-z (mm)	0.18 ± 0.17	0.15 ± 0.17	0.06 ± 0.24
3D-TP (%)	1.25 ± 0.42†	1.98 ± 0.78	1.90 ± 0.75
3D-TPx (%)	0.46 ± 0.92*	1.32 ± 1.11	1.39 ± 1.05
3D-TPy (%)	0.43 ± 0.54	0.66 ± 0.97	0.61 ± 0.75
3D-TPz (%)	0.37 ± 0.33	0.34 ± 0.40	0.14 ± 0.53
From neutral to the Patrick position			
3D-translation (mm)	1.17 ± 0.30	1.12 ± 0.39	1.97 ± 0.84**
3D-translation-x (mm)	−0.38 ± 0.40	−0.26 ± 0.56	−0.44 ± 0.63
3D-translation-y (mm)	−0.41 ± 0.41	−0.56 ± 0.34	−1.04 ± 0.51**
3D-translation-z (mm)	−0.86 ± 0.31	−0.68 ± 0.40	−1.40 ± 0.85**
3D-TP (%)	2.37 ± 0.60	2.58 ± 0.86	4.41 ± 1.81**
3D-TPx (%)	−0.76 ± 0.79	−0.60 ± 1.27	−0.97 ± 1.36
3D-TPy (%)	−0.85 ± 0.84	−1.29 ± 0.79	−2.33 ± 1.10**
3D-TPz (%)	−1.73 ± 0.63	−1.55 ± 0.91	−3.15 ± 1.86**

Values are mean ± standard deviation.
The direction of the connecting line between the FHC at the neutral position (the origin) and that at each other position was divided into a 3D vector, and each value of the *x*, *y*, and *z*-axis element was divided by the diameter of the femoral head, to produce 3D-TPx (%), 3D-TPy (%), and 3D-TPz (%). Each *x*, *y*, and *z*-axis pointed anteriorly, superiorly, and laterally, respectively.
* $P<0.05$ for the comparison between normal male hips and normal female hips.
† $P<0.01$ for the comparison between normal male hips and normal female hips.
‡ $P<0.05$ for the comparison between normal female hips and dysplastic hips.
** $P<0.01$ for the comparison between normal female hips and dysplastic hips.

Table III
Linear correlation coefficients among clinical and morphological parameters

	Normal male hips ($N=20$)	Normal female hips ($N=20$)	Dysplastic hips ($N=22$)
3D-migration			
Age	0.000	−0.113	−0.259
BMI	−0.321	−0.127	−0.067
CE angle	−0.206	−0.031	−0.349
Femoral head radius	−0.044	0.074	−0.127
Acetabular sphere radius	0.255	0.381	0.348
3D-MP			
Age	−0.019	−0.086	−0.324
BMI	−0.289	−0.112	−0.107
CE angle	−0.200	0.026	−0.293
Femoral head radius	−0.106	−0.067	−0.252
Acetabular sphere radius	0.203	0.262	0.243

There was no significant correlation at $P<0.05$.

respectively (Table VI). For the 3D-translation value and interobserver reproducibility, the ICC and the RMSE were 0.866 and 0.193 mm, respectively, and for the 3D-translation vector (*x*, *y*, *z*) the mean ICC and the mean RMSE were 0.921 and 0.209 mm, respectively.

Discussion

This study analyzed 3D morphology and 3D motions of the *in vivo* native hip with a non-invasive method using 3D MRI voxel-based registration technique. The present method had high reproducibility for evaluation of 3D-translation of the hip joint.

Developmental hip dysplasia shows acetabular coverage deficiency on a standard radiograph, and has been considered to have a tendency toward anterolateral migration of the femoral head[32]. However, there have been few investigations concerning the 3D distance between AC and FHC, namely 3D-migration in the present study. In computed tomography (CT)-based surface models, Murphy *et al.*[7] reported 3D-migration to be 4.7 ± 2.5 mm for dysplastic hips, 1.5 ± 1.1 mm for normal female hips, and 0.9 ± 0.3 mm for all normal hips. These results indicated the tendency that normal female hips have more 3D-migration than normal male hips. Pienkowski *et al.*[33] defined 3D-migration as joint incongruity and reported 3D-migration to be 3.0 ± 1.3 mm for Legg–Calvé–Perthes disease and 1.2 ± 0.5 mm for 10 normal male hips using MRI-based surface models. In these two studies, however, there was no information about the direction of 3D-migration. Although Gose *et al.*[34] reported that the FHC was located posteriorly, superiorly, and laterally compared with the AC in 123 (82%) of 150 cerebral palsy hips using CT-based surface models, there have been no publications regarding the direction of 3D-migration in dysplastic hips without spasticity. In the present study, CE angle was the determinant for 3D-migration ($\beta=-0.415$, $P=0.001$), and there was a statistical significant difference in 3D-migration between normal female hips and dysplastic hips ($P=0.047$). The FHC in the dysplastic hips tended to migrate superiorly. However, there were no statistical significant differences between the normal female hips and the dysplastic hips in 3D-migration-x/3D-MPx or 3D-migration-z/3D-MPz in the anteroposterior or mediolateral directions, respectively. This lack of differences may be attributed to the study design: all dysplastic hips in the present study were pre-OA or in the early stages. Further longitudinal 3D morphological analysis of dysplastic hips may reveal that the FHC of dysplastic hips migrates anteriorly and laterally at more advanced stages of OA.

There has been only one kinematic study regarding the hip joint center translation of the *in vivo* native hip[12]. In a MRI study based on a surface registration technique of extreme flexion of the hip in female professional dancers, Gilles *et al.* reported a mean translation of 2.12 ± 0.79 mm (0.57–4.10 mm) without evaluation of the translation direction[12]. In the present study, the FHC tended to translate antero-inferiorly from neutral to 45° flexion, anteriorly from neutral to 15° extension and postero-infero-medially from neutral to the Patrick position.

An interesting finding of the present study was that the dysplastic hip translated significantly further than the normal female hip from neutral to the Patrick position. Another interesting finding was that there was a significant correlation between the 3D-translation and the morphological data, and the CE angle of dysplastic hips exhibited the strongest correlation with the 3D-translation from neutral to the Patrick position ($P<0.001$; $r=-0.851$). The CE angle and 3D-translation in normal female hips were not correlated ($P=0.430$; $r=-0.187$). The multiple linear regression analyses also revealed that CE angle is the major determinant for 3D-translation from neutral to the Patrick position ($\beta=-0.730$, $P<0.001$). These results may indicate that hip instability is increased with decreasing CE angle <20°. Using skin marker accelerometry, Maeyama *et al.*[5] reported hip joint acceleration during the gait cycle was significantly larger in dysplastic than in normal hips. They also reported that the magnitude of acceleration significantly correlated with the CE angle ($r=-0.732$), in agreement with the present results. The present study also confirmed the findings of Maeyama *et al.* that the CE angle can predict hip joint instability[5].

It is also interesting that the FHC translated postero-infero-medially from neutral to the Patrick position. There have been a few reports that the femoral head translates anteriorly[9,35]. There have

Table IV
Linear correlation coefficients compared with 3D-translation and 3D-TP

	Normal male hips ($N = 20$)		Normal female hips ($N = 20$)		Dysplastic hips ($N = 22$)	
	3D-translation	3D-TP	3D-translation	3D-TP	3D-translation	3D-TP
From neutral to 45° flexion						
Age	0.508*	0.484*	0.250	0.297	0.393	0.337
BMI	0.093	0.140	−0.178	−0.174	0.104	0.064
CE angle	−0.157	−0.160	−0.397	−0.323	−0.509*	−0.482*
Femoral head radius	0.118	0.021	0.595**	0.468*	0.375	0.260
Acetabular sphere radius	0.071	−0.007	0.656**	0.558*	0.475*	0.403
3D-migration	0.285	0.294	0.167	0.174	0.443*	0.482*
3D-MP	0.277	0.292	0.089	0.115	0.377	0.430*
From neutral to 15° extension						
Age	0.164	0.143	0.520*	0.531*	0.400	0.338
BMI	0.335	0.366	0.508*	0.536*	0.619**	0.592**
CE angle	−0.018	−0.021	−0.298	−0.246	−0.178	−0.153
Femoral head radius	−0.119	−0.195	0.267	0.157	0.155	0.065
Acetabular sphere radius	−0.416	−0472*	0.358	0.260	0.367	0.310
3D-migration	−0.079	−0.076	0.092	0.085	0.100	0.122
3D-MP	−0.070	−0.062	0.054	0.063	0.080	0.113
From neutral to the Patrick position						
Age	0.227	0.196	0.146	0.168	0.171	0.114
BMI	0.311	0.376	−0.177	−0.183	0.344	0.329
CE angle	−0.102	−0.103	−0.187	−0.118	−0.851***	−0.835***
Femoral head radius	0.147	0.016	0.488*	0.369	0.238	0.152
Acetabular sphere radius	0.205	0.099	0.544*	0.447*	0.639**	0.583**
3D-migration	−0.238	−0.239	0.252	0.260	0.247	0.264
3D-MP	−0.247	−0.239	0.189	0.214	0.203	0.230

*$P < 0.05$; **$P < 0.01$; ***$P < 0.001$.

been no reports that the femoral head translates posteriorly, inferiorly or medially; such translation may cause posteroinferior or posterior lesions in the acetabulum. In femoroacetabular impingement, the first structure to fail could be the anterosuperior acetabular labrum[36,37]. Persistent anterosuperior abutment with chronic leverage of the head in the acetabulum may result in chondral injury in the posteroinferior acetabulum[36,37]. However, the mechanism that causes the sole posteroinferior or posterior labral or chondral lesion has not been elucidated, and could be shearing force or the direct contact causes the posterior or posteroinferior lesion in the Patrick position (flexion, abduction and external rotation). This study was the first to investigate the kinematics of the *in vivo* native hip in the Patrick position. The majority of labral or chondral lesions have been reported to be located at the anterior acetabulum. A sole posterior or posteroinferior lesion was reported in 4–7% of patients in an arthroscopic study[38] and in 5–9% of patients in surgical and MRI studies[39,40]. Hip kinematics in the Patrick position in the present study may be demonstrative of these lesions.

As a cause of translation of the FHC, the difference of curvature between the femoral head and acetabulum should be considered. The hip joint has traditionally been considered to be a ball and socket joint, which means the surfaces of the acetabulum and femoral head are congruent in any position[41]. However, it has been reported that both the acetabulum and the femoral head are not simply spherical[42–44], which would cause joint translations during normal hip movement. In the present study, subjects with deformed femoral heads were excluded, and there were no significant differences in the spherical geometry of the femoral head between normal hips and dysplastic hips. To our knowledge, however, the curvature of the acetabular cartilage surface in dysplasia has not been clarified. In order to elucidate the mechanism of hip joint translation, a comparison of the curvature of the acetabular cartilage surface in normal hips to dysplastic hips may be required.

As a second factor concerning femoral head translation, a few *in vitro* studies supported the concept that soft tissue damage around the hip (for example, the capsule, ligaments, and labrum) predisposes the hip joint to instability[9,10]. Crawford *et al.* concluded that the *in vitro* condition of loss of the labral seal is a critical event that leads to destabilization of the hip[9]. Because it is a commonly held view that labral tears of the acetabulum are caused by bony acetabular

Table V
Determinants of 3D-migration and 3D-translation from neutral to 45° flexion, 15° extension, and the Patrick position in all hips ($N = 62$)

Adjusted R^2	3D-migration			3D-translation from neutral to 45° flexion			3D-translation from neutral to 15° extension			3D-translation from neutral to the Patrick position		
	0.199			0.347			0.331			0.526		
	B	*β*	*P*	*B*	*β*	*P*	*B*	*β*	*P*	*B*	*β*	*P*
Age				0.014	0.370	0.001	0.007	0.205	0.084			
Sex (female)							0.381	0.560	<0.001			
Laterality	0.317	0.252	0.032									
BMI							0.052	0.438	0.002			
CE angle	−0.034	−0.415	0.001							−0.064	−0.730	<0.001
Femoral head radius												
Acetabular sphere radius				0.055	0.283	0.012						
3D-migration				0.198	0.340	0.003						

R^2, coefficient of determination; *B*, unstandardized regression coefficient; *β*, standardized partial regression coefficient.
Stepwise multiple linear regression analyses were used.

Table VI
Intra- and interobserver reproducibilities

Parameter	ICC	RMSE (mm)	Mean error of measurement (mm)
Observer 1			
3D-translation	0.912	0.151	0.046 ± 0.042
3D-translation-x	0.959	0.218	0.088 ± 0.058
3D-translation-y	0.961	0.147	0.025 ± 0.043
3D-translation-z	0.856	0.221	0.032 ± 0.064
Observer 2			
3D-translation	0.874	0.192	0.059 ± 0.054
3D-translation-x	0.937	0.242	0.076 ± 0.068
3D-translation-y	0.953	0.162	0.017 ± 0.047
3D-translation-z	0.887	0.202	0.014 ± 0.059
Interobserver			
3D-translation	0.866	0.193	0.052 ± 0.055
3D-translation-x	0.936	0.258	0.082 ± 0.072
3D-translation-y	0.956	0.157	0.021 ± 0.046
3D-translation-z	0.871	0.212	0.023 ± 0.062

RMSE, root mean square error of difference.
Values are including 95% confidence intervals of the mean error of measurement.

dysplasia[40,45], the present findings that translation increases with the decreasing CE angle are reasonable.

The possibility of the existence of an asymptomatic labral tear has been reported in morphologically normal hips of young volunteers, indicated by high signal intensity within the labrum with MRI[46,47]. Several investigators have also reported absent labrum in 2.5–14% of asymptomatic hips using MRI[46–49]. In the present study, there were several normal hips that exhibited a large amount of translation. Although these subjects may have had labral tear or absent labrum, the labral disorder could not be assessed using the modality of the current study. Further investigation into the relations between labral tears and hip translation may be required to clarify the pathomechanisms of hip changes before occurrence of symptoms and involvement of articular cartilage at an early phase of OA. In the future, using this technique in a longitudinal study, it may be evaluated whether instability causes disease progression not only in the dysplastic hip but also in the morphologically normal hip, particularly in primary OA.

There are two potential limitations in the present study. First, the study was based on static 3D MRI views of the hip at different positions, and the study included a limited number of hips. The static measurements could not evaluate any inertial or functional effects that might occur during activities of daily life. It would be reasonable to perform dynamic studies to supplement the findings of the current static study. Second, the 1 mm isotropic voxel may be low resolution for an accurate FHC location. Although obtaining MR images with high resolution is an effective way of minimizing volume-averaging effects, the present resolution was probably the minimal requirement for acquiring images with sufficient signal-to-noise ratio, using current MR equipment, and it was difficult for the patients to spend more time for MRI scanning. Nevertheless, because the RMSE for 3D-translation was within 0.2 mm, we concluded that the evaluation of hip joint translation using this novel method was validated.

In conclusion, the present study showed that the FHC translates postero-infero-medially from neutral to the Patrick position, and there is a significant strong negative correlation between the CE angle and 3D-translation from neutral to the Patrick position. These findings suggest that hip instability is increased in proportion to the severity of dysplasia. This new MRI technique obtained new information on the kinematics of the *in vivo* native hip without subjecting the participants to radioactive exposure. Hopefully this new information on the kinematics of the hip joint will assist clinicians in obtaining a better understanding of the hip joint and some of its disorders. Additionally, the present technique has a number of other potential applications. For example, 3D-translation from neutral to the Patrick position associated with hip joint stability or instability as a result of joint preserving surgery such as osteotomy and labral repair or with disease progression in OA could be studied. With further development, this technique may be useful in investigating 3D-translation of the hip with femoroacetabular impingement.

Author contributions

All authors were involved in drafting the article critically for important intellectual content, and all authors approved the content of the manuscript. Takashi Sakai had full access to all of the data in the study and takes responsibility for the integrity of the data and the accuracy of the data analysis.

Study conception and design: Keisuke Akiyama, Takashi Sakai, Kazuomi Sugamoto.

Acquisition of data: Keisuke Akiyama, Takashi Sakai.

Analysis and interpretation of data: Keisuke Akiyama, Takashi Sakai, Junichiro Koyanagi, Hideki Yoshikawa, Kazuomi Sugamoto.

Conflict of interest

All authors did not receive any financial and personal relationships with other people or organizations that could inappropriately influence (bias) our work.

Acknowledgments

The authors would like to thank Mr Yoshihiro Sakaguchi, Ms Naomi Dejima and Ms Tomoko Morita for obtaining MR images, Mr Ryoji Nakao, Dr Yukitaka Nagamoto and Dr Tsuyoshi Murase for technical support, Dr Katsuya Nakata for helpful advises, Ms Aya Sasaki and Ms Ai Shintaku for their help, and Mr Norio Sugimoto for statistical advises. This study was supported in part by Japanese Grant-in-Aid for Scientific Research (C) and Osaka gas group Welfare Foundation.

References

1. Murphy SB, Ganz R, Müller ME. The prognosis in untreated dysplasia of the hip. A study of radiographic factors that predict the outcome. J Bone Joint Surg Am 1995;77:985–9.
2. Jacobsen S, Sonne-Holm S, Søballe K, Gebuhr P, Lund B. Joint space width in dysplasia of the hip: a case-control study of 81 adults followed for ten years. J Bone Joint Surg Br 2005;87:471–7.
3. Mavcic B, Iglic A, Kralj-Iglic V, Brand RA, Vengust R. Cumulative hip contact stress predicts osteoarthritis in DDH. Clin Orthop Relat Res 2008;466:884–91.
4. Chegini S, Beck M, Ferguson SJ. The effects of impingement and dysplasia on stress distributions in the hip joint during sitting and walking: a finite element analysis. J Orthop Res 2009;27:195–201.
5. Maeyama A, Naito M, Moriyama S, Yoshimura I. Evaluation of dynamic instability of the dysplastic hip with use of triaxial accelerometry. J Bone Joint Surg Am 2008;90:85–92.
6. Engesaeter IØ, Lie SA, Lehmann TG, Furnes O, Vollset SE, Engesaeter LB. Neonatal hip instability and risk of total hip replacement in young adulthood: follow-up of 2,218,596 newborns from the Medical Birth Registry of Norway in the Norwegian Arthroplasty Register. Acta Orthop 2008;79:321–6.
7. Murphy SB, Kijewski PK, Millis MB, Harless A. Acetabular dysplasia in the adolescent and young adult. Clin Orthop Relat Res 1990;261:214–23.
8. Mavcic B, Pompe B, Antolic V, Daniel M, Iglic A, Kralj-Iglic V. Mathematical estimation of stress distribution in normal and dysplastic human hips. J Orthop Res 2002;20:1025–30.

9. Crawford MJ, Dy CJ, Alexander JW, Thompson M, Schroder SJ, Vega CE, *et al*. The biomechanics of the hip labrum and the stability of the hip. Clin Orthop Relat Res 2007;465:16–22.
10. Ito H, Song Y, Lindsey DP, Safran MR, Giori NJ. The proximal hip joint capsule and the zona orbicularis contribute to hip joint stability in distraction. J Orthop Res 2009;27:989–95.
11. Maeyama A, Naito M, Moriyama S, Yoshimura I. Periacetabular osteotomy reduces the dynamic instability of dysplastic hips. J Bone Joint Surg Br 2009;91:1438–42.
12. Gilles B, Christophe FK, Magnenat-Thalmann N, Becker CD, Duc SR, Menetrey J, *et al*. MRI-based assessment of hip joint translations. J Biomech 2009;42:1201–5.
13. Ishii T, Mukai Y, Hosono N, Sakaura H, Nakajima Y, Sato Y, *et al*. Kinematics of the upper cervical spine in rotation in vivo three-dimensional analysis. Spine 2004;29:139–44.
14. Goto A, Moritomo H, Murase T, Oka K, Sugamoto K, Arimura T, *et al*. In vivo elbow biomechanical analysis using magnetic resonance imaging. J Shoulder Elbow Surg 2004;13:441–7.
15. Moritomo H, Goto A, Sato Y, Sugamoto K, Murase T, Yoshikawa H. The truquetrum – hamate joint: an anatomic and in vivo three-dimensional kinematic study. J Hand Surg 2003;28:797–805.
16. Tönnis D, Berlin, etc. Die angeborene hüftdysplasie und hüftluxation im kindesund erwachsenenalter. Springer-Verlag; 1984. pp. 74–82.
17. Nishii T, Sugano N, Sato Y, Tanaka H, Miki H, Yoshikawa H. Three-dimensional distribution of acetabular cartilage thickness in patients with hip dysplasia: a fully automated computational analysis of MR imaging. Osteoarthritis Cartilage 2004;12:650–7.
18. Fredensborg N. The CE angle of normal hips. Acta Orthop Scand 1976;47:403–5.
19. Crowe JF, Mani VJ, Ranawat CS. Total hip replacement in congenital dislocation and dysplasia of the hip. J Bone Joint Surg Am 1979;61:15–23.
20. Sugano N, Nishii T, Takao M. The Asian hip. In: The Adult Hip. 2nd edn. Philadelphia: Lippincott Williams and Wilkins; 2006: 1060–77.
21. Quick HH, Ladd ME, Hoevel M, Bosk S, Debatin JF, Laub G, *et al*. Real-time MRI of joint movement with trueFISP. J Magn Reson Imaging 2002;15:710–5.
22. Holden M, Hill DL, Denton ER, Jarosz JM, Cox TC, Rohlfing T, *et al*. Voxel similarity measures for 3-D serial MR brain image registration. IEEE Trans Med Imaging 2000;19:94–102.
23. Takao M, Sugano N, Nishii T, Miki H, Koyama T, Masumoto J, *et al*. Application of 3D-MR image registration to monitor diseases around the knee joint. J Magn Reson Imaging 2005;22:656–60.
24. Patrick HT. Brachial neuritis and sciatica. JAMA 1917;29:2176–9.
25. Lorensen WE, Cline HE. Marching cubes: a high resolution 3D surface construction algorithm. Comput Graph (ACM) 1987; 21:163–9.
26. Drapikowski P. Surface modeling–uncertainty estimation and visualization. Comput Med Imaging Graph 2008;32:134–9.
27. Moritomo H, Murase T, Goto A, Oka K, Sugamoto K, Yoshikawa H. In vivo three-dimensional kinematics of the midcarpal joint of the wrist. J Bone Joint Surg Am 2006;88:611–21.
28. Maes F, Vandermeulen D, Suetens P. Comparative evaluation of multiresolution optimization strategies for multimodality image registration by maximization of mutual information. Med Image Anal 1999;3:373–86.
29. Grood ES, Suntay WJ. A joint coordinate system for the clinical description of three-dimensional motions: application to the knee. J Biomech Eng 1983;105:136–44.
30. Park MS, Kim SJ, Chung CY, Choi IH, Lee SH, Lee KM. Statistical consideration for bilateral cases in orthopaedic research. J Bone Joint Surg Am 2010;92:1732–7.
31. Bryant D, Havey TC, Roberts R, Guyatt G. How many patients? How many limbs? Analysis of patients or limbs in the orthopaedic literature: a systematic review. J Bone Joint Surg Am 2006;88:41–5.
32. Leunig M, Podeszwa D, Beck M, Werlen S, Ganz R. Magnetic resonance arthrography of labral disorders in hips with dysplasia and impingement. Clin Orthop Relat Res 2004;418: 74–80.
33. Pienkowski D, Resig J, Talwalkar V, Tylkowski C. Novel three-dimensional MRI technique for study of cartilaginous hip surfaces in Legg–Calvé–Perthes disease. J Orthop Res 2009;27:981–8.
34. Gose S, Sakai T, Shibata T, Murase T, Yoshikawa H, Sugamoto K. Morphometric analysis of acetabular dysplasia in cerebral palsy: three-dimensional CT study. J Pediatr Orthop 2009;29: 896–902.
35. Dy CJ, Thompson MT, Crawford MJ, Alexander JW, McCarthy JC, Noble PC. Tensile strain in the anterior part of the acetabular labrum during provocative maneuvering of the normal hip. J Bone Joint Surg Am 2008;90:1464–72.
36. Ganz R, Parvizi J, Beck M, Leunig M, Nötzli H, Siebenrock KA. Femoroacetabular impingement: a cause for osteoarthritis of the hip. Clin Orthop Relat Res 2003;417:112–20.
37. Beck M, Kalhor M, Leunig M, Ganz R. Hip morphology influences the pattern of damage to the acetabular cartilage: femoroacetabular impingement as a cause of early osteoarthritis of the hip. J Bone Joint Surg Br 2005;87:1012–8.
38. McCarthy JC, Noble PC, Schuck MR, Wright J, Lee J. The Otto E. Aufranc Award: the role of labral lesions to development of early degenerative hip disease. Clin Orthop Relat Res 2001; 393:25–37.
39. Neumann G, Mendicuti AD, Zou KH, Minas T, Coblyn J, Winalski CS, *et al*. Prevalence of labral tears and cartilage loss in patients with mechanical symptoms of the hip: evaluation using MR arthrography. Osteoarthritis Cartilage 2007;15: 909–17.
40. Wenger DE, Kendell KR, Miner MR, Trousdale RT. Acetabular labral tears rarely occur in the absence of bony abnormalities. Clin Orthop Relat Res 2004;426:145–50.
41. Hammond BT, Charnley J. The sphericity of the femoral head. Med Biol Eng 1967;5:445–53.
42. Bullough PG, Goodfellow JW, Greenwald AS, O'Connor JJ. Incongruent surfaces in the human hip joint. Nature 1968;217.
43. Menschik F. The hip joint as a conchoid shape. J Biomech 1997;30:971–3.
44. Gu D, Chen Y, Dai K, Zhang S, Yuan J. The shape of the acetabular cartilage surface: a geometric morphometric study using three-dimensional scanning. Med Eng Phys 2008;30: 1024–31.
45. Leunig M, Werlen S, Ungersbock A, Ito K, Ganz R. Evaluation of the acetabular labrum by MR arthrography. J Bone Joint Surg Br 1997;79:230–4.
46. Cotten A, Boutry N, Demondion X, Paret C, Dewatre F, Liesse A, *et al*. Acetabular labrum: MRI in asymptomatic volunteers. J Comput Assist Tomogr 1998;22:1–7.
47. Abe I, Harada Y, Oinuma K, Kamikawa K, Kitahara H, Morita F, *et al*. Acetabular labrum: abnormal findings at MR imaging in asymptomatic hips. Radiology 2000;216:576–81.
48. Lecouvet FE, Vande Berg BC, Malghem J, Lebon CJ, Moysan P, Jamart J, *et al*. MR imaging of the acetabular labrum: variations in 200 asymptomatic hips. Am J Roentgenol 1996;167: 1025–8.
49. Aydingöz U, Oztürk MH. MR imaging of the acetabular labrum: a comparative study of both hips in 180 asymptomatic volunteers. Eur Radiol 2001;11:567–74.